Surface Heterogeneity in Micropores of Pillared Clays: The Limits of Classical Pore-Filling Mechanisms

Laurent J. Michot,*,† Frédéric Villiéras,† Jean-François Lambert,‡ Latifa Bergaoui,‡,§ Yves Grillet,|| and Jean-Louis Robert⊥

Laboratoire "Environnement et Minéralurgie", I.N.P.L.-ENSG-CNRS URA 235, Rue du Doyen Roubault, BP40, 54501 Vandoeuvre Cedex, France, Laboratoire de Réactivité de Surface, Tour 54, UPMC, 4 Place Jussieu, 75252 Paris Cedex 05, France, Centre de Thermodynamique et de Microcalorimétrie CNRS 26, Rue du 141ème R.I.A., 13331 Marseille Cedex 03, France, and Centre de Recherches sur la Synthèse et la Chimie des Minéraux, CNRS, 1A, Rue de la Férollerie, 45071 Orléans Cedex 2, France

Received: November 6, 1997; In Final Form: February 22, 1998

The microporosity of Al_{13}-intercalated and -pillared synthetic saponites with variable layer charge (from 0.8 to 1.5 per unit cell) was studied by high-resolution quasi-equilibrium adsorption volumetry and low-temperature adsorption microcalorimetry. A strong positive correlation was observed between the adsorbed amounts of nitrogen and argon and the quantity of intercalated aluminum, suggesting that a simple micropore-filling mechanism is inappropriate to interpret N_2 and Ar adsorption on intercalated and pillared clays. Adsorption energy distributions were calculated using the derivative isotherm summation (DIS) procedure. They reveal that, at 77 K, nitrogen (and argon to a lesser extent) "titrates" the Brønsted acidic sites of the pillars and does not provide direct information about the liquid microporous volume between pillars. This picture of N_2 and Ar adsorption suggests a critical reexamination of many published data concerning the surface area and porous volume of pillared clays.

Introduction

Metal oxide pillared clays were first developed at the end of the 1970s.[1,2] They are obtained through the ionic exchange of smectite clays with metal polycations that intercalate between the clay layers. Generally, their structure is stabilized by heating in air at medium temperatures (≤500 °C). The presence of these pillars between the clay layers provides some acidic sites and yields a bidimensional porosity in the interlayer space. Both these properties make these materials attractive for catalytic[3] and environmental[4,5] applications. Various precursors of different elements including iron,[6] titanium,[7] and gallium[8] were used as pillaring agents. The most common inorganic pillar is the aluminum polycation with Keggin structure $[Al_{13}O_4(OH)_{24+x}(H_2O)_{12-x}]^{(7-x)+}$ known as the "Al_{13} unit" and obtained from the hydrolysis of aluminum chloride and nitrate:[9,10] it is also one of the few instances in which the structure of the pillaring species is precisely known.

One interesting prospect in the synthesis of pillared clays materials is that their porosity should be tailorable both in total volume and pore size by varying either the charge density of the clay layer or the charge of the intercalant. In fact, in the case of clays with octahedral substitution, the charge density of the host layer can be varied by using the so-called Hoffmann−Klemen effect.[11] The starting clay is partially exchanged with lithium and heated to 250 °C. Lithium migrates in the octahedral layer and saturates some charges. Such a procedure was used by Boyd and co-workers[12] in the case of organo-clays. Other ways of varying the charge density is to use synthetic clays such as flurorohectorite[13,14] or saponites.[15−17] Recently, we obtained some preliminary results on the porosity of a series of pillared saponites with systematically varying layer charges, using carbon dioxide and nitrogen adsorption.[16] The microporous volumes derived from the Dubinin−Radushkevich plots based on CO_2 adsorption were equal to theoretical micropore volumes estimated from the amount of aluminum intercalated. However, nitrogen "surface areas" did not follow the same trend but actually *increased* with the pillar density in the interlayer, indicating that a micropore-filling mechanism is not suited to explain nitrogen adsorption in this type of materials. With regard to the importance of porosity characterization for environmental or catalytic applications, the issue of what is actually measured by nitrogen adsorption is extremely important. In the present paper, we study in detail the adsorption of nitrogen and argon on Al_{13}-pillared saponites with varying charge density using a quasi-equilibrium volumetric procedure[18−20] and low-temperature adsorption microcalorimetry. As will be shown, the results have a broader significance concerning the interpretation of nitrogen (and other gases) adsorption data for a large category of inorganic materials.

Experimental Section

Synthesis. Synthetic saponites were prepared by hydrothermal synthesis at 400 °C under a 1000 bar water pressure, with run durations of 4 weeks, in Morey type externally heated pressure vessels. The samples were insulated from the vessel wall by a silver coating. The starting products were gels of appropriate compositions, prepared by coprecipitation of Na, Mg, Al, and Si hydroxides at pH = 14, according to the gelling method of Hamilton and Henderson.[21] The source of Na was sodium carbonate, the sources of Al and Mg were titrated

† Laboratoire "Environnement et Minéralurgie".
‡ Laboratoire de Réactivité de Surface.
§ Current address: Laboratoire de Chimie des Matériaux et Catalyze Hétérogène, Campus Universitaire, 1060 le Belvédère, Tunis, Tunisie.
|| Centre de Thermodynamique et de Microcalorimétrie CNRS 26.
⊥ Centre de Recherches sur la Synthèse et la Chimie de Minéraux.

S1089-5647(98)00110-2 CCC: $15.00
Published on Web 04/14/1998

solutions of their nitrates, and the source of Si was $(C_2H_5O)_4Si$ (TEOS). Prior to hydrothermal synthesis, the starting product was dried and calcined and then crushed for further homogenization. After the hydrothermal synthesis, the sample was quenched and examined by X-ray diffraction and ^{29}Si and ^{27}Al NMR to confirm the single-phase character. The resulting structural formula is $Na_x(Si_{8-x},Al_x)(Mg_6)O_{20}(OH)_4$, with $0.8 \leq x \leq 1.5$. The sodium form of the synthetic saponites will be referred to as SNa-*x*, where *x* is the negative layer charge, per unit cell. The cationic exchange capacities (CEC) of the samples were determined by exchanging the cations with the cobaltihexamine ion $[Co(NH_3)_6]^{3+}$.[22] In all cases there is an excellent match between the theoretical and experimental values.

The saponite pillaring method has been described elsewhere.[15] The Al_{13}- intercalated products will be referred to as SI-*x*, where *x* is the substitutional charge per unit cell as given in the above formula, and the pillared products obtained after calcination at 500 °C will be referred to as SP-*x*.

Methods

X-ray Diffraction. X-ray diffraction patterns were recorded on a Siemens D500 diffractometer using the Cu Kα_1 radiation. The *d*001 spacings were measured at the 001 line maximum.

Argon and Nitrogen Adsorption. Low-pressure isotherms of argon and nitrogen were recorded on a lab-built automatic quasi-equilibrium volumetric setup.[18,19] In this method a slow, constant and continuous flow of adsorbate was introduced into the adsorption cell. From the recording of quasi-equilibrium pressures vs time, the adsorption isotherms were derived. The experimental conditions were a sample mass of ≈0.1 g, outgassing at 0.001 Pa at a temperature of 150 °C. The data were then treated using the improved derivative isotherm summation (DIS) procedure designed by Villiéras et al.[19,20] to examine the surface heterogeneity of the samples. Due to the large number of experimental data points acquired by the quasi-equilibrium procedure, the experimental derivative of the adsorbed quantity as a function of the logarithm of relative pressure can be calculated accurately. The total derivative adsorption isotherm on a heterogeneous surface is simulated by the sum of local theoretical derivative adsorption isotherms on heterogeneous surfaces with random heterogeneity.

$$\theta_t = \sum_i X_i \theta_{it} = X_i \int_\Omega \theta_i(\epsilon)\, \chi_i(\epsilon)\, d\epsilon \qquad (1)$$

where θ_t is the total adsorption isotherm, θ_{it} are the adsorption isotherms on the different energetic domains of the surface, X_i is its contribution to θ_t, ϵ is the adsorption energy, Ω is the physical domain of ϵ, $\theta_i(\epsilon)$ is a "local" theoretical adsorption isotherm, and $\chi_i(\epsilon)$ is the dispersion of ϵ on the *i*th domain. The theoretical isotherms used[20] are obtained by first approximating the energy distribution by the condensation approximation (CA). For describing adsorption into micropores, a generalization of the Dubinin−Asthakov isotherm was proposed:

$$\theta_{it}(P/P_0) = \exp\left[-\left[\frac{kT}{E_i}\ln\left(\frac{P_i^0}{P}\right)\right]^{r_i}\right. \qquad (2)$$

where E_i is the variance of $\chi_i(\epsilon)$ and r_i is a parameter governing the shape of the distribution function. For $r_i = 2$, eq 2 becomes the Dubinin−Radushkevich isotherm. In practice, in application of the Dubinin−Astakhov equation, P_i^0 is commonly identified with the saturated vapor pressure P_s. If this approximation may be justified in some cases, P_i^0 can generally not be identified with P_s and must be treated as a best fit parameter that represents the pressure at which the largest micropores of the family are filled. Equation 2 can be extended to take into account the effect of lateral interactions ω by replacing $(kT/E)\ln(p^0/p)$ by $\Delta = (kT/E)\ln(p^0/p) - \omega\theta/E$).

The derivatives of eq 2 are

$$\left[\frac{\partial\theta_t}{\partial \ln p}\right]_T = \frac{r\frac{kT}{E}[\Delta]^{r-1}\theta}{\left(1 - \frac{r\omega}{E}[\Delta]^{r-1}\theta\right)} \qquad (3)$$

It is a Gaussian-like function widened on the low-energy side for $r_i < 3$ and widened on the high-energy side for $r_i > 3$.

The expression of the second derivative is relatively complicated and is obtained through a numerical procedure. In the DIS method, the identification of the different parameters is obtained from the coordinates of the maximum and from the width of the derivative. The mathematical relations between E_i, r_i, and P_i^0 can be easily derived from the expression of the first and second derivatives of eq 2 when the second derivative equals zero. When the parameter corresponding to lateral interactions is taken equal to 0, a simple expression can be obtained:

$$\frac{E}{kT} = \ln\left(\frac{p^0}{p^*}\right)\left[\frac{r\ln(p^0/p^*)}{r-1}\right]^{1-r} \qquad (4)$$

Then, for given values of r and p^0, the amount adsorbed on the domain *i*, X_i, can be obtained from the comparison between the height of the experimental and calculated maxima at P^*:

$$X_i = \frac{(dV_{ads}/d\ln(P^*/P_s)}{d\theta_i/d\ln(P^*/P_s)} \qquad (5)$$

In practice, r_i and P_i^0 are fixed, and from the position of a maximum P^*, the adsorption capacity X_i and E_i are calculated. r_i and P_i^0 are adjusted until the simulated curve matches the experimental curve.

A multilayer extension of eq 3 has also been proposed in order to simulate peaks corresponding to multilayer adsorption, i.e., adsorption on external surfaces.[20] From this model, it is possible to extract the contribution of the first adsorbed layer. The multilayer adsorption isotherm is written:

$$\theta_{it}(P) = (1 + P)\theta_{i1}(P) \qquad (6)$$

where θ_{i1} corresponds to the adsorption of the first layer and is calculated using eq 3 with P defined as follows:

$$P = \frac{p/p_s}{1 - k'(p/p_s)} \qquad (7)$$

where k' is generally chosen equal to 1. The first derivative of eq 7 is written:

$$\left[\frac{\partial\theta_t}{\partial \ln p}\right]_T = \left[\frac{(P+1)^2 r\Delta^{r-1}\left(\frac{kT}{E}\right)}{1 - \left(\frac{\omega}{E}\right)r\Delta^{r-1}e^{-\Delta^r}} + P(P+1)\right]e^{-\Delta r} \qquad (8)$$

In this case, the experimental parameters corresponding to the different domains are obtained in the same way as from eq 2. In some cases, especially for low-energy adsorption domains,

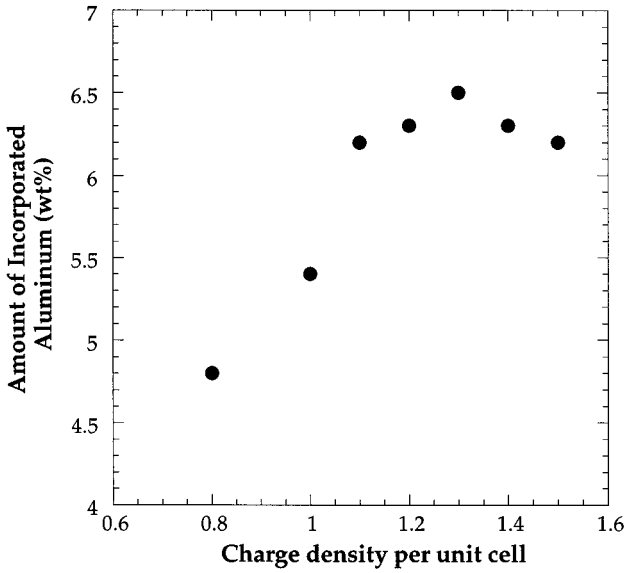

Figure 1. Evolution with the saponites layer charge of the quantities of aluminum fixed on intercalation.

the maxima are not observed. If an inflection point can be determined, the parameters are calculated from the inflection point properties in the same way as for a maximum. Finally, if no inflection point appears, i.e., if r_i is close to 1, all the parameters must be adjusted. This is accomplished by choosing a point on the derivative curve; parameters are adjusted step by step in order to calculate the derivative going through this point and properly matching the experimental curve.

Further combination of the obtained results yields the condensation curves which can be corrected to energy distribution for each adsorption domain by applying the Rudzinski−Jagiello correction.[23]

$$\theta_{1t} = \int_{\Omega} \theta_1(\epsilon)\, \chi(\epsilon)\, d\epsilon = -X(\epsilon_c) - \frac{\Pi^2}{6}(kT)^2 \left(\frac{\partial \chi}{\partial \epsilon}\right)_{\epsilon=\epsilon_c} \quad (9)$$

Low-Temperature Argon and Nitrogen Adsorption Microcalorimetry. Low-temperature adsorption microcalorimetry[24] allows a simultaneous recording of the adsorption isotherm and the corresponding derivative enthalpy. For that purpose, the adsorbate is introduced into the adsorption cell at a slow and constant flow rate, under quasi-equilibrium conditions. The adsorption cell is surrounded by an isothermal calorimeter kept at 77 K by total immersion in a liquid nitrogen bath. Both the quasi-quilibrium pressure and the heat flow, resulting from adsorption, are recorded simultaneously. The evolution of the heat of adsorption vs surface coverage can then be obtained. In the present study 150 mg samples were outgassed at 150 °C, prior to each experiment.

Results

Amount of Aluminum Incorporated. Figure 1 presents the quantity of aluminum incorporated in the clay as a function of the charge density of the layer host. The amount increases linearly up to a charge density of 1.3 per half unit cell and remains constant thereafter.[25] This limiting value observed for the interlayer pillars density can be related to steric constraints in solution: it corresponds rather well to a close packing of Al_{13} polycations in two dimensions, considering the radius of the hydrated polycation in solution.

X-ray Diffraction. Figure 2 presents typical X-ray diffraction patterns obtained for the saponite with a layer charge of

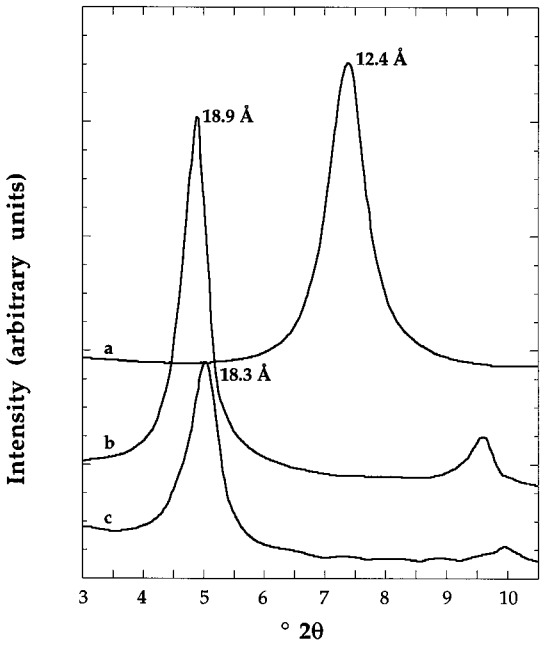

Figure 2. X-ray diffraction patterns of (a) **S−Na-1.1**, (b) **SI-1.1**, and (c) **SP-1.1**.

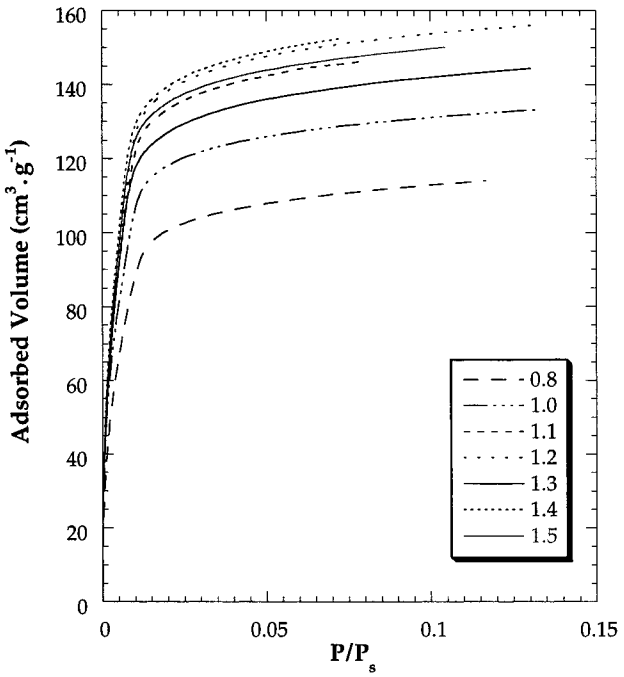

Figure 3. Argon adsorption isotherms at 77 K on Al_{13}-intercalated saponites. Outgassing conditions: 150 °C, 0.001 Pa.

1.1. The starting sample exhibits a *d*(001) line corresponding to an interlayer distance of 12.5 Å. Upon intercalation the interlayer distance increases to a value of 18.9 Å. It decreases slightly after calcination at 500 °C to 18.3 Å.

Argon Adsorption. *Intercalated Samples.* Figure 3 presents the argon adsorption isotherms, measured after outgassing the samples at 150 °C, for relative pressures ≤ 0.15. The adsorbed volumes increase with charge density up to a value of 1.2 and remain more or less constant for higher densities. This pattern seems to follow the amount of aluminum adsorbed. This correspondence appears more strikingly when plotting the BET surface area as a function of charge density as displayed in Figure 4. Except for sample **SI-1.3**, the curve follows exactly the one displayed in Figure 1 concerning the amount of

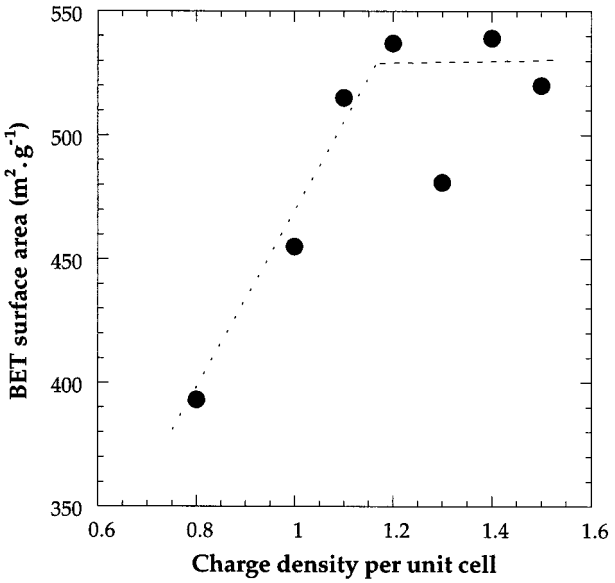

Figure 4. Evolution with the layer charge of the argon BET surface areas of Al_{13}-intercalated saponites.

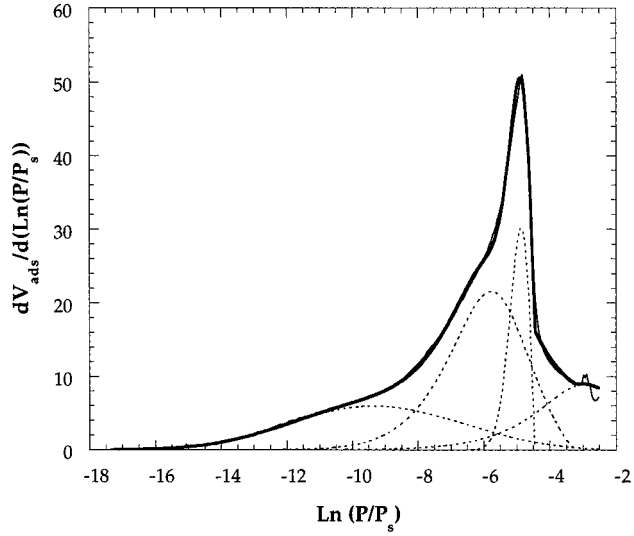

Figure 5. Derivative argon adsorption isotherm together with its decomposition using the derivative isotherm summation (DIS) method: sample **SI-1.1**.

aluminum incorporated: "surface areas" from argon BET are positively correlated with the pillar density in the interlayer. Furthermore, the adsorbed volumes and surface areas appear very high at around 540 m^2/g, considering the amount of micropores that should be left between the pillars inside the interlayer space.

Similarly, a positive correlation of N_2 BET "surface areas" with interlayer pillar density observations has been previously made for pillared saponites.[16] However, the maximum value for surface areas was significantly lower in this case, at 420 m^2/g.

A typical derivative argon adsorption isotherm together with its decomposition using the derivative isotherm summation (DIS) method is presented in Figure 5 for sample **SI-1.1**. Table 1 presents the different parameters derived from the decomposition of the isotherms on the seven intercalated samples. All the derivative curves display the same pattern: they can be fitted by four theoretical derivative adsorption isotherms. The three at high energy are Dubinin−Astakhov isotherms, whereas the fourth one at low energy takes into account multilayer formation.

TABLE 1: Argon Adsorption at 77 K on Saponites with Varying Charge Density Intercalated with Al_{13} Polycations[a]

layer charge	domain	$\ln(P/P_s)$	model	r	$\ln(P^0/P_s)$	ω/kT	E/kT	V_m ($cm^3\ g^{-1}$)
0.8	1	−10.09	DA	5	−4	0	6.7	16.4
	2	−5.84	DA	2.15	−2.1	1.2	4.1	53.0
	3	−4.76	DA	2.1	−4.15	0	0.8	18.3
	4	−3.15	MDA	1.9	0	1.2	6.0	24.9
1.0	1	−10.01	DA	4	−3	0	6.0	29.3
	2	−5.79	DA	2.2	−2	1.2	4.1	58.0
	3	−4.78	DA	1.9	−4.35	0	0.6	18.2
	4	−2.82	MDA	1.9	0	1.1	4.4	25.8
1.1	1	−9.70	DA	3.8	−1.5	0	8.9	34.7
	2	−5.74	DA	2.15	−2.1	1.2	3.9	68.0
	3	−4.83	DA	1.9	−4.4	0	0.6	22.4
	4	−2.93	MDA	1.9	0	1.2	3.8	24.7
1.2	1	−9.5	DA	3.8	−1.5	0	8.7	34.4
	2	−5.76	DA	2.35	−2	1.1	4.0	69.1
	3	−4.89	DA	1.9	−4.45	0	0.6	27.6
	4	−2.82	MDA	1.9	0	1.2	3.6	22.7
1.3	1	−9.5	DA	3.7	−1.5	0	8.7	33.0
	2	−6	DA	2.4	−2.1	1.1	4.1	56.1
	3	−5.03	DA	1.9	−4.5	0	0.8	22.6
	4	−3.15	MDA	1.9	0	1.2	4.3	29.4
1.4	1	−9.1	DA	3.3	−1.5	0	8.4	42
	2	−5.96	DA	2.4	−2.1	1.1	4.1	63.1
	3	−5.0	DA	1.9	−4.5	0	0.7	26.4
	4	−3.0	MDA	1.9	0	1.3	3.7	23.6
1.5	1	−9.8	DA	4.4	−1.5	0	8.8	32.6
	2	−5.89	DA	2.3	−2.1	1.1	4.1	70.3
	3	−4.98	DA	1.9	−4.5	0	0.7	23.6
	4	−2.92	MDA	1.9	0	1.2	3.8	23.6

[a] Set of parameters obtained from the application of the DIS method in which the Dubinin−Asthakov equation is applied to adsorption in micropores (DA) and its multilayer extension is applied to external surfaces (MDA). Outgassing conditions: 150 °C, 0.001 Pa.

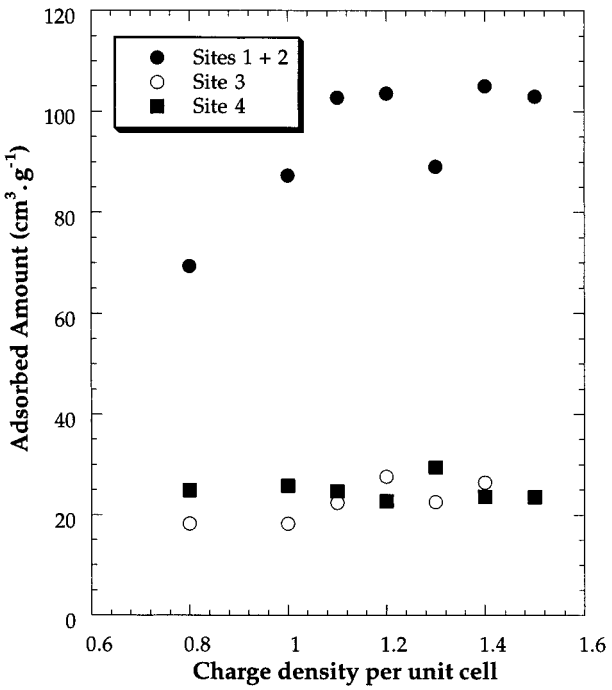

Figure 6. Evolution with the charge density of the host layer of the adsorbed volumes on the different sites of Al_{13}-intercalated saponites obtained from the DIS procedure. Argon adsorption at 77 K.

The first two domains in the high-energy range appear rather heterogeneous, as evidenced by the high value of the parameter E/kT. On the contrary, the third peak centered around $\ln(P/P_s) = -5$ is extremely sharp. Figure 6 presents the evolution of the adsorbed volumes on the different sites as a function of the charge density of the host layer. Due to their high heterogeneity,

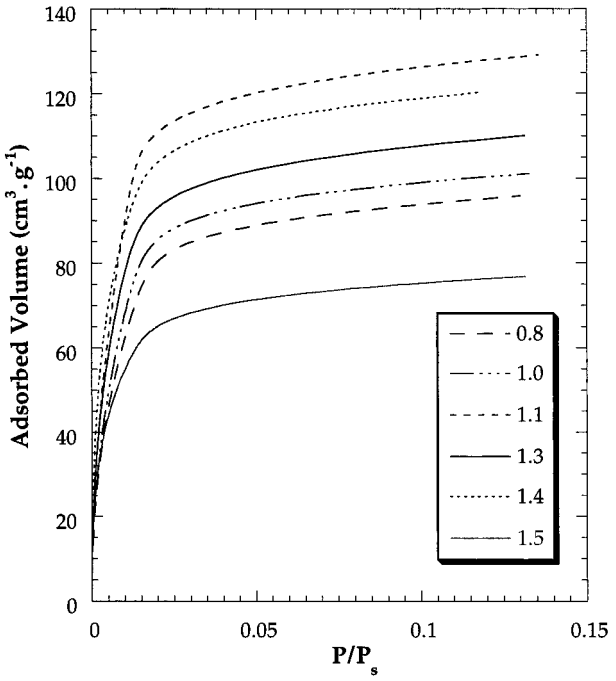

Figure 7. Argon adsorption isotherms at 77 K on Al_{13}-pillared saponites. Outgassing conditions: 150 °C, 0.001 Pa.

sites 1 and 2 were considered together in this plot. It appears that the volume of argon adsorbed on these two sites, when plotted against layer charge x, follows the pattern already observed for the quantity of intercalated aluminum and for the BET surface areas: initial linear increase followed by a plateau. The trend is not so clear for the volumes adsorbed on site 3: they possibly follow a similar pattern, taking into account that sample **SI-1.3** is probably aberrant. On the contrary, the volumes adsorbed on site 4 seem to slightly decrease with increasing charge density. As usual, sample **SI-1.3** does not fit in the series.

Pillared Samples. Figure 7 presents the argon adsorption isotherms obtained on pillared samples. These curves exhibit the same pattern as the ones obtained in the case of intercalated samples: the adsorbed amount increases up to a layer charge of 1.1 and remains nearly constant for higher values. However, sample **SP-1.5** adsorbs much less argon.

Figure 8 presents a typical derivative argon adsorption isotherm (sample **SP-1.1**) together with its DIS decomposition, whereas Table 2 presents the different parameters derived from the decomposition of the isotherms on the six pillared samples. As in the case of intercalated samples, four peaks fit the derivative isotherm quite well. The position of the low energy peak around $\ln(P/P_s) = -3$ does not change upon calcination. On the contrary, the three peaks at higher energy are shifted toward lower energy. For all sites, the amount of argon adsorbed on a given pillared sample is generally lower than that adsorbed on its intercalated counterpart. The tendencies observed for the amounts of argon adsorbed on the different sites are compatible with those for intercalated samples if sample **SP-1.5** is ignored, as illustrated in Figure 9.

Nitrogen Adsorption. Four samples with $x = 0.8$, 1.1, 1.3, and 1.5 were selected to study nitrogen adsorption.

Intercalated Samples. Figure 10 presents the nitrogen adsorption isotherms obtained for the four samples in the range of relative pressures < 0.15. The pattern observed mimics the one obtained when argon is used as an adsorbate: the adsorbed volumes increase up to $x = 1.3$.

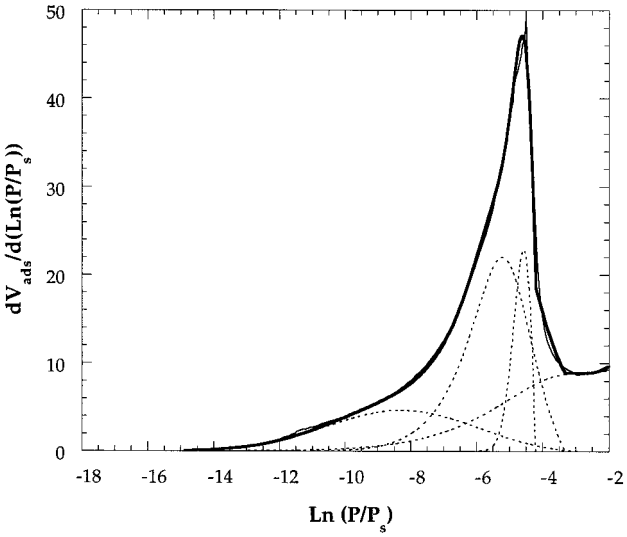

Figure 8. Derivative argon adsorption isotherm together with its decomposition using the derivative isotherm summation (DIS) method: sample **SP-1.1**.

TABLE 2: Argon Adsorption at 77 K on Saponites with Varying Charge Density Pillared with Al_{13} Polycations[a]

layer charge	domain	$\ln(P/P_s)$	model	r	$\ln(P^0/P_s)$	ω/kT	E/kT	V_m ($cm^3\,g^{-1}$)
0.8	1	−8.48	DA	3.2	−1.5	0	7.8	20.6
	2	−5.24	DA	2.3	−1.9	1.1	3.5	35.2
	3	−4.35	DA	1.9	−3.9	0	0.7	11.5
	4	−2.87	MDA	1.9	0	1.1	4.4	24.5
1.0	1	−8.83	DA	3.6	−1	0	8.6	22.2
	2	−5.25	DA	2.4	−1.9	1	3.5	36.7
	3	−4.48	DA	2	−4	0	0.7	12.5
	4	−2.96	MDA	1.9	0	1.1	4.6	26.7
1.1	1	−8.3	DA	3	−2.7	0	6.4	25.2
	2	−5.2	DA	2.15	−2.1	1.2	3.2	52.4
	3	−4.57	DA	1.9	−4.2	0	0.5	15.0
	4	−2.86	MDA	1.9	0	1.1	4.4	31.8
1.3	1	−9.0	DA	3.7	−1.5	0	6.4	24.5
	2	−5.57	DA	2.4	−1.9	1	3.9	47.5
	3	−4.56	DA	1.9	−4	0	0.8	14.3
	4	−2.88	MDA	1.9	0	1.2	3.6	21.3
1.4	1	−9.4	DA	3.9	−1.3	0	8.7	29.3
	2	−5.65	DA	2.4	−1.9	1	4	52.3
	3	−4.45	DA	1.9	−4	0	0.7	11.3
	4	−3.01	MDA	1.9	0	1.2	4	25.2
1.5	1	−9.8	DA	4.5	−1.2	0	9.1	16.1
	2	−5.65	DA	2.3	−1.9	1	4	38.0
	3	−4.4	DA	1.9	−3.9	0	0.7	7.0
	4	−2.82	MDA	1.9	0	1.2	3.5	14.6

[a] Set of parameters obtained from the application of the DIS method in which the Dubinin−Asthakov equation is applied to adsorption in micropores (DA) and its multilayer extension is applied to external surfaces (MDA). Outgassing conditions: 150 °C, 0.001 Pa.

Figure 11 presents a typical derivative nitrogen adsorption isotherm (**SI-1.1**) together with its DIS decomposition. The shape of the derivative isotherm is very different from that observed in the case of argon adsorption. For all the derivative isotherms, no less than seven domains are needed for a good fit. Additional peaks appear in the high energy range whereas the very sharp peak observed around $\ln(P/P_s) = -5kT$ in the case of argon adsorption is absent. Table 3 presents the decomposition results obtained for the four intercalated samples under study. Each decomposition results in four high-energy adsorption domains ($\ln(P/P_s) < -11kT$), two medium energy domains ($-8kT < \ln(P/P_s) < -5kT$), and one low-energy domain located around $\ln(P/P_s) = -3.6kT$. Figure 12 exhibits the evolution of the adsorbed volumes corresponding to each of these three energy ranges. For the high- and medium-energy

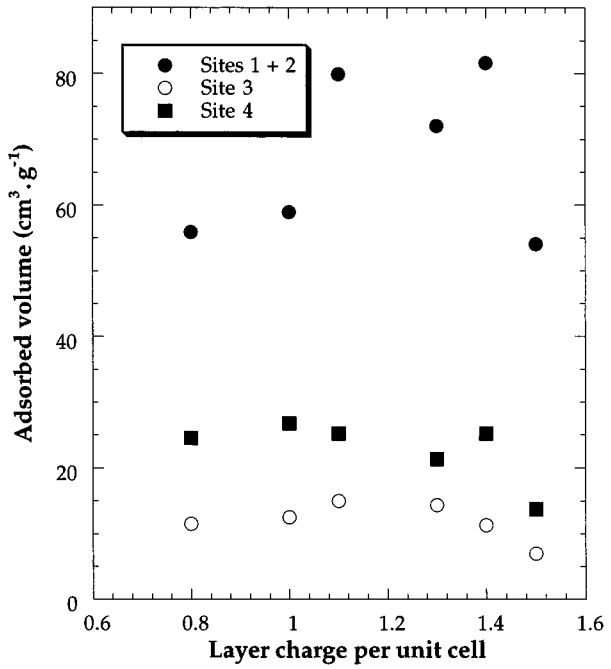

Figure 9. Evolution with the charge density of the host layer of the adsorbed volumes on the different sites of Al_{13}-pillared saponites obtained from the DIS procedure. Argon adsorption at 77 K.

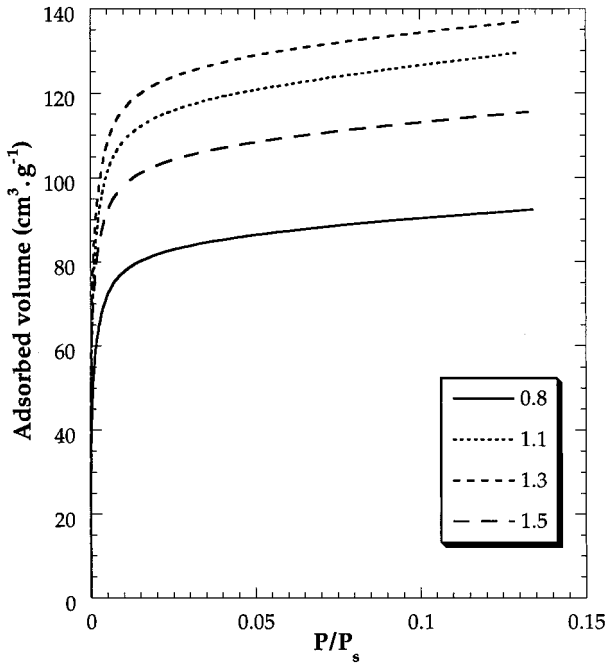

Figure 10. Nitrogen adsorption isotherms at 77 K on Al_{13}-intercalated saponites. Outgassing conditions: 150 °C, 0.001 Pa.

domains, the adsorbed quantities increase with layer charge up to $x = 1.3$ and decrease for **SI-1.5**. The quantities adsorbed in the low-energy domain appear roughly constant with layer charge.

Pillared Samples. Only limited results are available for N_2 adsorption in pillared samples. Some differences with the corresponding intercalated samples seem to be present here. The peaks we previously defined as "high-energy" are significantly shifted toward lower energies, and the corresponding adsorbed volumes are reduced. The fitting parameters for the different site families are found in Table 4. The volumes adsorbed in the low-energy domain appear nearly constant between different

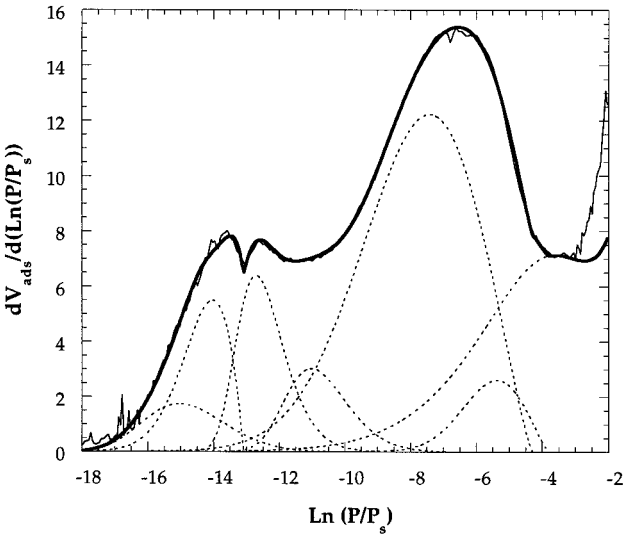

Figure 11. Derivative nitrogen adsorption isotherm together with its decomposition using the derivative isotherm summation (DIS) method: sample **SP-1.1**.

TABLE 3: Nitrogen Adsorption at 77 K on Saponites with Varying Charge Density Intercalated with Al_{13} Polycations[a]

layer charge	domain	ln(P/P_s)	model	r	ln(P^0/P_s)	ω/kT	E/kT	V_m (cm^3 g^{-1})
0.8	1	−15.68	DA	5	−9	0	7.0	3.8
	2	−14.28	DA	1.75	−13.3	0	1.6	7.2
	3	−12.93	DA	9.5	−7.0	0	6.0	6.2
	4	−11.53	DA	8	−6.0	0	5.6	2.5
	5	−7.42	DA	2.2	−4	0	4.5	42.1
	6	−5.40	DA	2.2	−3.8	0	2.1	2.4
	7	−3.74	MDA	2.0	0	1	5.3	23.8
1.1	1	−15.03	DA	5	−9.5	0	5.8	5.3
	2	−14.03	DA	1.8	−13.1	0	1.5	10.0
	3	−12.71	DA	10	−6.0	0	6.8	11.7
	4	−11.02	DA	7	−5.0	0	6.1	7.1
	5	−7.41	DA	2.2	−4.3	0	4.1	54.8
	6	−5.37	DA	2.2	−3.8	0	2.1	5.9
	7	−3.61	MDA	2.0	0	1.1	4.8	28.9
1.3	1	−15.84	DA	7	−7.2	0	8.8	3.1
	2	−13.68	DA	1.7	−13.0	0	1.2	12.7
	3	−12.60	DA	8.5	−8.0	0	5.2	15.5
	4	−11.04	DA	6	−6.0	0	5.2	9.7
	5	−7.47	DA	2.3	−4.3	0	4.1	51.8
	6	−5.37	DA	2.3	−4	0	1.8	9.6
	7	−3.33	MDA	2.0	0	1	5.0	28.9
1.5	1	−15.69	DA	3	−12	0	4.2	2.2
	2	−13.01	DA	1.6	−12.2	0	1.5	18.2
	3	−12.04	DA	11	−8.5	0	3.6	3.8
	4	−11.40	DA	6	−7.0	0	4.5	5.9
	5	−7.89	DA	2.3	−4.2	0	4.7	48.0
	6	−5.43	DA	2.2	−4.0	0	1.9	5.0
	7	−3.69	MDA	2.0	0	1	5.2	27.4

[a] Set of parameters obtained from the application of the DIS method in which the Dubinin−Asthakov equation is applied to adsorption in micropores (DA) and its multilayer extension is applied to external surfaces (MDA). Outgassing conditions: 150 °C, 0.001 Pa.

samples, whereas the volumes for the medium- and high-energy domains increase up to a layer charge of 1.1 and decrease thereafter.

Discussion

Adsorption on External Surfaces. All the experimental results available suggest that argon and nitrogen adsorption in aluminum-intercalated or -pillared saponites cannot be explained by a classical micropore-filling mechanism. Indeed, the trend observed is exactly opposite to what would be foreseen by the

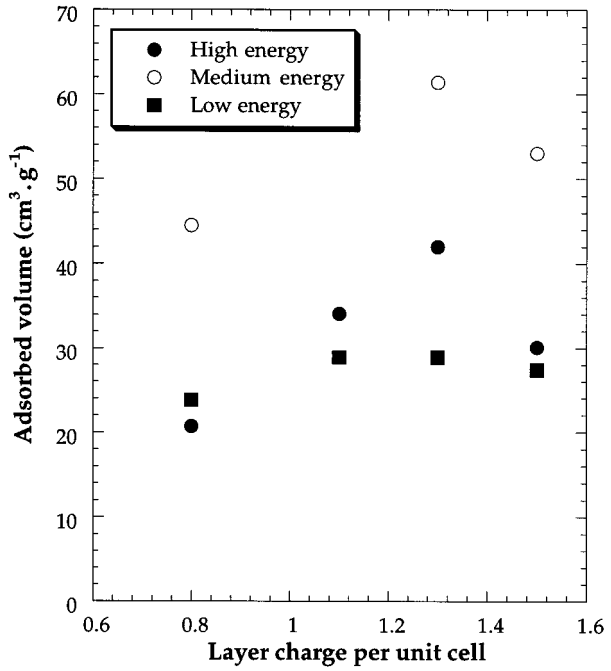

Figure 12. Evolution with the charge density of the host layer of the adsorbed volumes on the different sites of Al_{13}-intercalated saponites obtained from the DIS procedure. Nitrogen adsorption at 77 K.

TABLE 4: Nitrogen Adsorption at 77 K on Saponites with Varying Charge Density Pillared with Al_{13} Polycations[a]

layer charge	domain	$\ln(P/P_s)$	model	r	$\ln(P^0/P_s)$	ω/kT	E/kT	V_m ($cm^3\ g^{-1}$)
0.8	1	−14.07	DA	7	−7	0	7.2	2.5
	2	−12.72	DA	3.6	−10.5	0	2.4	5.0
	3	−11.10	DA	5	−5.0	0	6.4	14.1
	4	−9.06	DA	4	−5.0	0	4.4	8.0
	5	−6.66	DA	2.3	−4.3	0	3.1	41.9
	6	−4.68	DA	2.3	−3.7	0	1.3	3.4
	7	−3.64	MDA	1.9	0	1.3	4.8	25.9
1.1	1	−13.77	DA	1.7	−13.0	0	1.4	4.1
	2	−12.64	DA	9	−6.0	0	6.7	7.9
	3	−10.47	DA	4.8	−5.0	0	5.7	12.5
	4	−8.76	DA	4	−5.0	0	4.0	8.5
	5	−6.54	DA	2.3	−4.5	0	2.6	41.7
	6	−4.74	DA	2.4	−3.8	0	1.2	7.3
	7	−3.34	MDA	1.9	0	1.2	4.6	27.3
1.3	1	−14.25	DA	5	−5.0	0	9.7	4.8
	2	−13.02	DA	1.8	−12.1	0	1.4	6.8
	3	−11.97	DA	6	−9.0	0	3.1	4.0
	4	−10.77	DA	4	−5.0	0	6.2	8.8
	5	−7.23	DA	2.4	−4.0	0	4.0	19.9
	6	−5.19	DA	2.3	−4.0	0	1.5	1.0
	7	−4.32	MDA	1.9	0	1.2	6.0	26.4
1.5	1	−14.31	DA	7	−5.0	0	9.5	4.2
	2	−12.84	DA	1.7	−12.2	0	1.1	5.1
	3	−11.97	DA	6	−9.0	0	3.1	3.3
	4	−10.56	DA	4	−5.0	0	6.0	9.8
	5	−6.93	DA	2.4	−4.0	0	3.7	23.1
	6	−4.68	DA	2.2	−3.7	0	1.3	1.3
	7	−3.60	MDA	1.9	0	1.1	5.7	21.8

[a] Set of parameters obtained from the application of the DIS method in which the Dubinin−Asthakov equation is applied to adsorption in micropores (DA) and its multilayer extension is applied to external surfaces (MDA). Outgassing conditions: 150 °C, 0.001 Pa.

micropore-filling model: the adsorbed quantities increase with the number of pillars, i.e., with decreasing micropore space. Furthermore, important differences between argon and nitrogen derivative adsorption isotherms are observed.

Whatever the adsorbate used and the layer charge of the sample, the low energy peak observed on all the decompositions exhibits similar characteristics and extension. As mentioned in the Experimental Section, it can be tentatively assigned to the adsorption of gas molecules on the external surfaces of clay particles. In the frame of this assumption, a value for the external surface area of approximately 100 $m^2\ g^{-1}$ is obtained. It is easily calculated that this value corresponds to stacks of around eight saponites sheets. The latter value is in good agreement with X-ray diffraction results.[25]

TABLE 5: Argon Adsorption at 77 K on Saponites with Varying Charge Density Intercalated with Al_{13} Polycations[a]

layer charge	domain	$\ln(P/P_s)$	number of Ar molecules per pillar
0.8	1	−10.09	5.4
	2	−5.84	17.3
	3	−4.76	6.0
1.0	1	−10.01	8.5
	2	−5.79	16.8
	3	−4.78	5.3
1.1	1	−9.70	8.8
	2	−5.74	17.2
	3	−4.83	5.7
1.2	1	−9.5	8.6
	2	−5.76	17.2
	3	−4.89	6.9
1.3	1	−9.5	8.0
	2	−6	13.5
	3	−5.03	5.4
1.4	1	−9.1	10.4
	2	−5.96	15.7
	3	−5.0	6.6
1.5	1	−9.8	8.2
	2	−5.89	17.8
	3	−4.98	6.0

[a] Adsorbed amounts on high- and medium-energy domains expressed as number of argon molecules per Al_{13} pillar.

High- and Medium-Energy Adsorption: Al_{13}-Intercalated Clays. If the low-energy peak is assigned to the external surface area of the clay platelets, the other peaks oberved on the decomposition of the derivative adsorption isotherms must be attributed to adsorption in the "gallery", or interlayer space of the intercalated and pillared saponites. On the basis of recent studies,[26,27] it seems reasonable to assume that, before calcination, most of the aluminum present in the interlayer space of saponites is under the form of Al_{13} polycations with Keggin structure. Indeed, ^{27}Al NMR experiments,[25,27] definitely show that this is the only polycation present in the Al solutions that we used for pillaring. At the hydrolysis ratio used in our work ($r = 2.2$), the formula of the polycation can be written as $[Al_{13}O_4(OH)_{26}(H_2O)_{10}]^{5+}$, which also matches the chemical analyses data. It is then possible to express adsorption results as numbers of molecules adsorbed per Al_{13} pillar, a presentation strongly suggested by the correlation between adsorbed gas amounts and pillar density.

Table 5 presents the results of such calculations, based on the data presented in Table 1 for Ar adsorption in intercalated saponites. The adsorption peaks are identified from their $\ln(P/P_s)$ values; the other decomposition parameters are found in Table 1. It appears that, for all samples but one (**SI-0.8**), the most energetic peak corresponds to the adsorption of eight to nine argon molecules per Al_{13} pillar. The second peak generally corresponds to the adsorption of 17 argon molecules (except for **SI-1.3**), and the third peak always accounts for approximately six molecules per pillar.

In the case of nitrogen adsorption, the same treatment can be applied (Table 6). For the evaluation, the high-energy peaks were lumped together as mentioned earlier in the text, and so were the medium energy peaks. It appears that the high-energy domains correspond to the adsorption of 6 to 9 nitrogen

TABLE 6: Nitrogen Adsorption at 77 K on Saponites with Varying Charge Density Intercalated with Al_{13} Polycations[a]

layer charge	domains	number of N_2 molecules per pillar
0.8	1+2+3+4	6.4
	5+6	14.5
1.1	1+2+3+4	8.6
	5+6	15.3
1.3	1+2+3+4	9.9
	5+6	14.8
1.5	1+2+3+4	7.6
	5+6	13.4

[a] Adsorbed amounts on high- and medium-energy domains expressed as number of argon molecules per Al_{13} pillar.

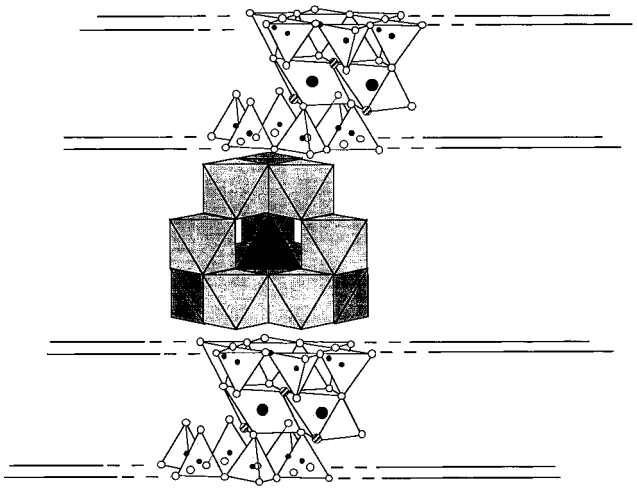

Figure 13. Schematic diagram of the interlayer of Al_{13}-intercalated saponites.

molecules per pillar, whereas the medium-energy domains represent 13 to 15 molecules per pillar.

The near constancy of these results most likely implies that *argon and nitrogen molecules adsorb on specific sites carried by the pillars*, rather than in the voids between pillars. In the case of nitrogen the high-energy sites are not all energetically equivalent, as four domains are needed in the decomposition to account for the adsorption of nitrogen molecules. In the case of argon, in contrast, one single domain (although with a high-energy dispersion, $E/kT > 8$) is sufficient to describe the adsorption on these sites.

It may be possible to go further in the characterization of these specific adsorption sites. Since the Al_{13} pillars are known to be oriented in the clay galleries with their C_3 axis perpendicular to the layers,[28] it can be seen that nine aluminum octahedra are located next to the layers (Figure 13). It is tempting to identify these "corner" sites with the high-energy sites observed in the decomposition of the derivative adsorption isotherms for argon and nitrogen sorption. Indeed, in the structure of pristine Al_{13} polycations, each octahedral Al bears a terminal OH_2 ligand, an essential feature in determining the Brønsted acidity of intercalated and pillared clays.[3,25,29] The importance of Brønsted acidity in nitrogen sorption is discussed further.

The medium-energy domain corresponding to 17 and 14 gas molecules for argon and nitrogen, respectively, is tentatively assigned to further adsorption on the pillar surfaces (on less specific sites). In that case, due to the difference in size between the two molecules, more argon than nitrogen should adsorb per pillar. This is actually the case, and the ratio of the number of argon atoms to nitrogen molecules (17/14 = 1.21) matches the ratio of the cross sectional area of these two molecules on hydroxylated surfaces (16.2/13.8 = 1.17).

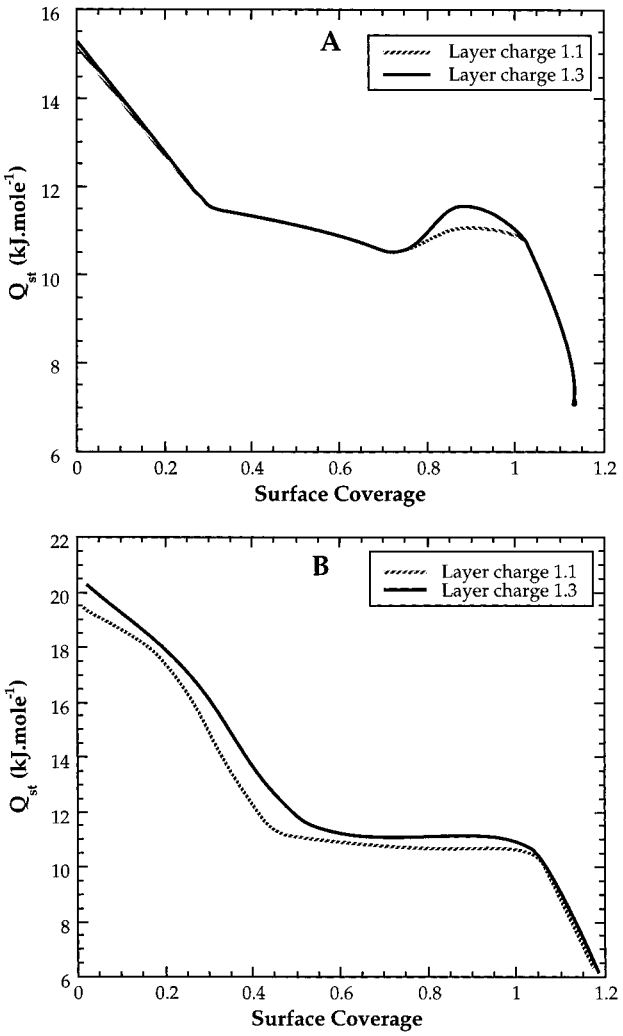

Figure 14. Evolution with surface coverage of the isosteric heat of adsorption of (a) argon and (b) nitrogen on samples **SI-1.1** and **SI-1.3**.

The low-energy domain observed only in the case of argon and exhibiting a very sharp peak in the derivative isotherm could indicate a rearrangement of argon molecules in order to accommodate more adsorbate in the galleries.

To confirm these assignments, low-temperature adsorption calorimetry experiments were carried out using both argon and nitrogen as adsorbates. Figure 14 presents the evolution with surface coverage of the isosteric heat of adorption for argon and nitrogen in the case of samples **SI-1.3** and **SI-1.1**. For both adsorbates, the curves do not look like those typical of microporous materials such as zeolites[30] or fibrous clay minerals,[31,32] as there is no plateau indicative of micropore filling at low surface coverage. The isosteric heat of adorption for nitrogen displays much higher adsorption energies than that for argon, in agreement with the results obtained by the DIS method.

Sample **SI-1.3** exhibits a slightly higher heat of nitrogen adsorption than **SI-1.1**. The curves for argon adsorption on the two samples are nearly superimposed except at coverages between 0.75 and 1. For a coverage of around 0.75, there is an increase in the heat of argon adsorption: this demonstrates a conformational change of argon molecules for accommodating more molecules in the available space, as already suggested by the argon adsorption isotherms. This change appears more marked for the sample with the higher layer charge. In view

TABLE 7: Argon Adsorption at 77 K on Saponites with Varying Charge Density Pillared with Al_{13} Polycations[a]

layer charge	domain	$\ln(P/P_s)$	number of Ar molecules per pillar
0.8	1	−8.48	6.7
	2	−5.24	11.5
	3	−4.35	3.8
1.0	1	−8.83	6.4
	2	−5.25	10.6
	3	−4.48	3.6
1.1	1	−8.3	6.4
	2	−5.2	13.2
	3	−4.57	3.8
1.3	1	−9.0	5.9
	2	−5.57	11.5
	3	−4.56	3.5
1.4	1	−9.4	7.3
	2	−5.65	13.0
	3	−4.45	2.8
1.5	1	−9.8	4.1
	2	−5.65	9.6
	3	−4.4	1.8

[a] Adsorbed amounts on high- and medium-energy domains expressed as number of argon molecules per Al_{13} pillar.

of the low intensity of this transition, it seems more likely due to a rearrangement of molecules than to a real phase transition. For all layer charges, this transition involves the adsorption of about six argon molecules per pillar, suggesting that it is occurring at the pillar surface rather than in the space between pillars. In our previous paper, dealing with CO_2 adsorption on the same samples, we indicated that a radius of around 0.8 nm for the intercalated Al_{13} units provides a good match between experimental and calculated values for the micropore volumes. The Al_{13} moiety can then be modeled in first approximation as a cylinder 1.6 nm in diameter and 0.9 nm in height (the latter value from X-ray data), having a surface area of 4.52 nm^2. Assuming that the cross-sectional area of argon molecules on hydroxylated surfaces is 0.138 nm^2,[33] a close hexagonal arrangement of argon molecules at the pillar surface would correspond to 33 argon molecules. For most samples (Table 5), one observes a total adsorption of 31 to 33 molecules per pillar. Therefore, the configuration of argon molecules after rearrangement would be very similar to a close packing on the pillar surface. The fact that the transition of rearrangement is not observed in the case of nitrogen is probably due to the stronger gas−solid interactions in this case, although differences in size between argon and nitrogen molecules may play a role too.

High- and Medium-Energy Adsorption: Al_{13}-Pillared Clays. As shown in the Results section the derivative adsorption isotherms obtained for pillared samples exhibit patterns similar to those observed for intercalated samples. For both argon and nitrogen, the volume of gas adsorbed on the low-energy domain is nearly constant and approximately equal to the corresponding value for intercalated samples (Tables 2 and 4). For the other energetic domains, the adsorbed volumes also seem to follow the pattern of the amount of incorporated aluminum. Tables 7 and 8 show that, except in the case of the sample with the highest charge, 6 to 7 argon molecules, 11 to 13 argon molecules, and roughly 4 argon molecules are adsorbed per pillar for the high-, medium-, and low-energy domains, respectively. In the case of nitrogen, the two samples with low charge density (0.8 and 1.1) yield comparable results of 6 to 7 and 15 to 17 nitrogen molecules per pillar on the high- and medium-energy domains, respectively. Sample **SP-1.5** is aberrant, but this may simply be due to the notorious difficulty in synthesizing pillared clays in a reproducible manner; in particular, the organization

TABLE 8: Nitrogen Adsorption at 77 K on Saponites with Varying Charge Density Pillared with Al_{13} Polycations[a]

layer charge	domains	number of N_2 molecules per pillar
0.8	1+2+3	7.0
	4+5+6	17.4
1.1	1+2+3	6.2
	4+5+6	14.5
1.3	1+2+3+4	5.9
	5+6	5.0
1.5	1+2+3+4	6.3
	5+6	6.1

[a] Adsorbed amounts on high- and medium-energy domains expressed as number of argon molecules per Al_{13} pillar.

of a pillared clay may be strongly perturbed by irregularities in the temperature ramp at the temperature of pillar-layer cross-linking.[34]

Thus, the results obtained for pillared samples indicate a picture globally similar to that for intercalated samples. Quantitative interpretation is, however, not easy. Indeed, important structural changes occur upon calcination of intercalated clays with tetrahedral charge defects. The exact structure of the pillars after calcination is not yet fully understood. The high-energy sites correspond to the adsorption of six to seven gas molecules and are difficult to assign precisely. They could still be "corner" sites, as in the case of intercalated samples, although in smaller amounts. In the case of nitrogen, the medium-energy sites correspond to the adsorption of approximately the same number of molecules as for intercalated clays (≈15) as for intercalated samples, but in the case of argon less molecules are adsorbed. The size reduction of the pillar in the *c* direction shown by X-ray diffraction could possibly explain this difference. Argon molecules still seem to undergo a conformational change, as a very sharp peak corresponding to the adsorption of four molecules per pillar is still present in the decomposition of derivative isotherms.

Implications for the Evaluation of Surface Areas of Pillared Materials. The above results underline the need for a reexamination of the exact nature of adsorbate/surface interaction in routinely performed measurements of surface areas and porosities by the physisorption of "inert" gases such as nitrogen and argon.

Nitrogen is in fact a weak Brønsted base: recent research has shown[35,36] that on acidic solids such as zeolites N_2 is adsorbed at 83 K through formation of an acid−base adduct with surface OH groups. The loss of the inversion center makes N−N stretching of adsorbed N_2 observable in IR, with a small blue shift indicating σ-bonding. Density functional calculations have confirmed the theoretical possibility of such an interaction, with an interaction energy of 0.157 eV, i.e., 15.1 kJ/mol; therefore, N_2 may be considered as a specific probe of strong Brønsted acid groups, being better suited to that use than stronger bases such as pyridine.

In pillared clays at 77 K, the strongest Brønsted acidic centers are the terminal H_2O ligands on the octahedral Al's of the pillars.[3] This provides a rationale for the above assignment of the strong N_2 adsorption sites to "corner sites", which are then equated to some of the terminal H_2O on the Al octahedra of the Al_{13} pillars. Furthermore, the isosteric heats of nitrogen adsorption (in the strong adsorption region: see Figure 14) are rather close to the theoretical interaction energies derived for N_2/zeolites. Why the strongest adsorption sites should be those H_2O groups in the immediate vicinity of the clay layers remains an open question; some type of cooperative interaction of adsorbed N_2 with the layers is probably involved.

The argon results are at first more puzzling. Argon can hardly be considered as a base, and yet it seems to exhibit a stronger interaction with the same sites responsible for nitrogen sorption. However, weak adducts of argon with strong acids such as HCl[37,38] and HF[39] and even with H_2O[40] have been widely studied in the gas phase. The interaction energies are between 1.2 and 2.1 kJ/mol for strong acids, i.e., much lower than the isosteric heats of argon adsorption observed on pillared saponites (Figure 14). Thus, interaction with acidic centers is not the main component of the energy of argon interaction with the surface: nevertheless, it represents a nonnegligible additional component that might cause preferential adsorption in the vicinity of acidic centers, all other things being equal. This additional acido-basic component is overcome at high argon coverages and reorganization occurs. Such an interpretation is confirmed by very recent infrared studies of argon adsorption at 100 K on a H−ZSM5 zeolite[41] that reveal an interaction of argon molecules with Brønsted acid sites.

We may now discuss the practical significance of the above findings. Pillared layered compounds are one of the major categories of materials synthesized by soft chemistry methods, and the success of a pillaring procedure is generally judged from two criteria: an increase in the interlayer spacing corresponding to basal planes (as seen from XRD) and an increase in the surface area of the materials, as estimated from N_2 "physisorption" using the BET equation. The latter measurement may only be taken as a technological indicator (the higher the BET surface area, the better the procedure), but problems arise when quantitative interpretation of the results is attempted.

Some studies still try to estimate a theoretical surface area by summing up the lateral surface of the pillars with the unoccupied surface of the interlayers. This calculation is obviously wrong since it neglects the excluded volume of the adsorbed molecule; the same molecule may be in contact with the pillar and the interlayer at the same time.

It is then logical to use a pore-filling model, and since in pillared clays the interlayer spacing corresponds roughly to the thickness of two nitrogen molecules, it is generally considered that there is a monolayer adsorption on both limiting surfaces of the interlayer, i.e., that nitrogen physisorption measures the accessible surface of the opened up clay layers (after subtracting the projection of the pillars on the surface). Corrections have been proposed for packing density variations in constrained spaces.[42,43]

In light of the results presented here, this view must be considered as wrong as well. This is not due to the existence of a rather strong interaction between nitrogen molecules and some specific surface sites, but to the marked heterogeneity in the distribution of such sites: they are located exclusively at the interface between pillars and clay layers. One of the basic assumptions of the BET model then breaks down, and it is not exaggerated to state that nitrogen adsorption at 77 K (and Ar adsorption to a lesser extent) is indeed a "pillars titration", not a measurement of exposed layers' surface area. Our suggestion to obtain a correct estimate of the exposed layer surface is to use CO_2 sorption instead, since this molecule does not exhibit specific interactions with pillared clay surface groups.[16]

Layer rigidity effects extensively discussed by Pinnavaia, Solin, and co-workers[44] could also be put forward to explain our results. Low charge intercalated clays would then exhibit a more corrugated behavior, and then less space would be available for gas adsorption. In view of the layer charges of the host layers studied, we think that this parameter can only play a minor role. Furthermore, the X-ray diffraction patterns of all samples are very similar with very well-defined 001 lines and exhibit in most cases many higher order reflections up to the sixth or eighth order. Therefore layer bending seems rather unlikely in our case.

Conclusion

The present study allows us to rationalize previously unexplained results of nitrogen adsorption data in pillared clays, especially the apparent increase in N_2 BET surface areas in series of samples where the available interlayer space actually decreases. The use of the DIS method suggests that at 77 K nitrogen adsorption on Al_{13}-intercalated and -pillared clays involves three successive phenomena in clearly separated energy ranges: (1) strong adsorption of N_2 molecules on Brønsted acidic terminal (H_2O) groups of the pillars in contact with the clay layers, up to nine molecules per pillar; (2) adsorption on remaining surface groups of the pillars, up to 14 molecules per pillar, leaving little or no free space in the interlayers; (3) weak, multilayer adsorption on the external surface of the pillared clays.

In the case of argon sorption, the same three phenomena are observed, but in view of the much weaker interaction of Ar with Brønsted acidic sites, a reorganization of the adsorbate may take place at $\theta \cong 0.75$ to accommodate more argon atoms in the interlayer.

This picture of N_2 and Ar adsorption suggests a critical reexamination of many published data on the surface area and porous volume of pillared clays. Contrary to a central assumption of the BET theory, the exposed surface of these materials is highly heterogeneous at the molecular scale since Brønsted acidic centers are present only on the pillars, and N_2 adsorption at low partial pressures is mostly dependent on the number of pillars, rather than on the available surface of propped up layers.

Furthermore, this study shows the potential of the DIS method in the evaluation of surface heterogeneity, especially when used in combination with other techniques such as microcalorimetry.

References and Notes

(1) Vaughan, D. E. W.; Lussier, R. J. *Preprints of the 5th International Conference on Zeolites*; Naples, Italy, June 2−6, 1980.

(2) Lahav, N.; Shani, U.; Shabtai, J. *Clays Clay Miner.* **1978**, *26*, 107.

(3) Lambert, J. F.; Poncelet, G. *Top. Catal.* **1997**, *4*, 43.

(4) Bergaoui, L.; Lambert, J. F.; Suquet, H.; Che, M. *J. Phys. Chem.* **1995**, *99*, 2155.

(5) Bergaoui, L.; Lambert, J. F.; Suquet, H.; Che, M. *J. Chim. Phys.* **1995**, *92*, 1486.

(6) (a) Burch, R.; Warburton, C. I. *Appl. Catal.* **1987**, *33*, 395. (b) Doff, D. H.; Gangas, N. H. J.; Allan, J. E. M.; Coey, J. M. D. *Clay Miner.* **1988**, *23*, 367. (c) Lee, W. Y.; Raythata, R. H.; Tatarchuk, B. J. *J Catal.* **1989**, *115*, 159. (d) Rightor, E. G.; Tzou, M.; Pinnavaia, T. J. *J Catal.* **1991**, *130*, 29. (e) Zhao, D.; Wang, G.; Yang, Y.; Guo, X.; Wang, Q.; Ren, J. *Clays Clay Miner.* **1993**, *41*, 317. (f) Lourvanij, K.; Rorrer, G. L. *Appl. Catal. A* **1994**, *109*, 147. (g) Jamis, J.; Drljaca, A.; Spiccia, L.; Smith, T. D. *Chem. Mater.* **1995**, *7*, 2086.

(7) (a) Sterte, J. *Clays Clay Miner.* **1986** *34*, 658. (b) Del Castillo, H. L.; Grange, P. *Appl. Catal. A* **1993**, *103*, 23. (c) Lin, J.-T.; Jong, S.-J., Cheng, S. *Microporous Mater.* **1993**, *1*, 287. (d) Jamis, J.; Drljaca, A.; Spiccia, L.; Smith, T. D. *Chem. Mater.* **1995**, *7*, 2086. (e) Swarnakar, R.; Brandt, K. B.; Kydd, R. A. *Appl. Catal. A* **1996**, *142*, 61. (f) Bovey, J. Kooli, F., Jones, W. *Clay Miner.* **1996**, *34*, 501.

(8) (a) Bellaloui, A.; Plee, D.; Meriaudeau P. *Appl. Catal.* **1990**, *63*, L7. (b) Bradley, S. M.; Kydd, R. A. *Catal. Lett.* **1991**, *8*, 185. (c) Bradley, S. M.; Kydd, R. A. *J. Catal.* **1993**, *141*, 239. (d) Bradley, S. M.; Kydd, R. A. *J. Catal.* **1993**, *142*, 448. (e) Gonzalez, F.; Pesquera, C.; Benito, I.; Mendioroz, S. *J. Chem. Soc., Chem. Commun.* **1991**, 578. (f) Gonzalez, F.; Pesquera, C.; Blanco, C.; Benito, I.; Mendioroz, S. *Inorg. Chem.* **1992**, *31*, 727. (g) Hernando, M. J.; Pesquera, C.; Blanco, C.; Benito, I.; Gonzalez, F. *Chem. Mater.* **1996**, *8*, 727. (h) Tang, X.; Xu, W. Q.; Shen, Y. F.; Suib, S. L. *Chem. Mater.* **1995**, *7*, 102.

(9) Bottero, J. Y.; Cases, J. M.; Fiessinger, F.; Poirier, J. E. *J. Phys. Chem.* **1980**, *84*, 2933.

(10) Bottero, J. Y.; Axelos, M. A.; Tchoubar, D.; Cases, J. M.; Fripiat, J. J.; Fiessinger, F. *J. Colloid Interface Sci.* **1987**, *117*, 47.
(11) Hofmann, U.; Klemen, R. *T. Anorg. Chem.*, **1950**, *262*, 95.
(12) Jaynes, W. F.; Boyd, S. A. *Clays Clay Miner.* **1991** *39*, 428.
(13) Barrer, R. M. *Clays Clay Miner.* **1989** *37*, 385.
(14) Butruille, J. R.; Michot, L. J.; Barrès, O.; Pinnavaia, T. J. *J. Catal.* **1993**, *139*, 664.
(15) Bergaoui, L.; Lambert, J. F.; Frank, R.; Suquet, H.;, Robert, J. L. *J. Chem. Soc., Faraday Trans.* **1995**, *91*, 2229.
(16) Bergaoui, L.; Lambert, J. F.; Vicente-Rodriguez, M. A.; Michot, L. J.; Villiéras, F. *Langmuir* **1995**, *11*, 2849.
(17) Grandjean, J.; Robert, J. L. *J. Colloid Interface Sci.* **1997**, *187*, 267.
(18) Michot, L.; François, M.; Cases, J. M. *Langmuir* **1990**, *6*, 677.
(19) Villiéras, F.; Cases, J. M., François, M.; Michot, L. J.; Thomas, F. *Langmuir* **1992**, *8*, 1789.
(20) Villiéras, F.; Michot, L. J.; Bardot, F.; Cases, J. M., François, M.; Rudzinski, W. *Langmuir* **1997**, *13*, 1104.
(21) Hamilton, D. L.; Henderson, C. M. B. *Miner. Mag.* **1968**, *36*, 832.
(22) Remy, J. C.; Orsini, L. *Sci. Sol.* **1976**, *4*, 269−275.
(23) Rudzinski, W.; Everett, D. H. *Adsorption of Gases on Heterogeneous Surfaces*; Academic Press: London, 1991.
(24) Rouquerol, J. *Calorimétrie d'Adsorption aux Basses Températures. I. Thermochimie*; CNRS Publications: Paris, 1972.
(25) Bergaoui, L. Ph.D. Thesis, Université de Paris VI, 1994.
(26) Schoonheydt, R. A.; Leeman, H.; Scorpion, A.; Lenotte, I.; Grobet, P. *Clays Clay Miner.* **1994** *42*, 518.
(27) Lambert, J.-F.; Chevalier, S.; Frank, R.; Suquet, H.; Barthomeuf, D. *J. Chem. Soc., Faraday Trans.* **1994**, *90*, 675.
(28) Nazar, L. F.; Liblong, S. W.; Yin, X. T. *J. Am. Chem. Soc.* **1991**, *113*, 5889.
(29) Mrad, I.; Ghorbel, A.; Tichit, D.; Lambert, J.-F. *Appl. Catal.*, in press.
(30) Grillet, Y.; Llewellyn, P. L.; Kenny, M. B.; Rouquerol, F.; Rouquerol, J. *Pure Appl. Chem.* **1993**, *65*, 2157.
(31) Grillet, Y.; Cases, J. M.; François, M.; Rouquerol, J.; Poirier, J. E. *Clays Clay Miner.* **1988** *39*, 191.
(32) Cases, J. M.; Grillet, Y.; François, M.; Michot, L.; Villiéras, F.; Yvon, J. *Clays Clay Miner.* **1991** *36*, 233.
(33) Rouquerol, J. Thèse de Doctorat d'Etat, Paris, 1965.
(34) Chevalier, S.; Frank, R.; Suquet, H.; Lambert, J.-F.; Barthomeuf, D. *J. Chem. Soc., Faraday Trans.* **1994**, *90*, 667.
(35) Neyman, K. M.; Strodel, P.; Ruzankin, S. Ph.; Schlensog, N.; Knözinger, H.; Rösch, N. *Catal. Lett.* **1995**, *31*, 273.
(36) Wakabayashi, F.; Fujino, T.; Kondo, J. N.; Domen, K.; Hirose, C. *J. Phys. Chem.* **1995**, *99*, 14805.
(37) Hutson, J. H. *J. Phys. Chem.* **1992**, *96*, 4237.
(38) Schröder, T.; Schinke, R.; Mandziuc, M.; Bacic, Z. *J. Chem. Phys.* **1994**, *100*, 7239.
(39) Hutson, J. H. *J. Phys. Chem.* **1992**, *96*, 6752.
(40) Germann, T. C.; Gutowsky, H. S. *J. Chem. Phys.* **1993**, *98*, 5235.
(41) Wakabayashi, F.; Kondo, J. N.; Domen, K.; Hirose, C. *J. Phys. Chem.* **1996**, *100*, 4154.
(42) Bergaya, F.; Gatineau, L.; Van Damme, H. In *multifunctional Mesoporous Inorganic Solids*; Sequeira, C. A. C., Hudson, M. J., Eds.; NATO ASI Series; Springer: New York, 1993; p 19.
(43) Ge, Z.; Li, D.; Pinnavaia, T. J. *Microporous Mater.* **1994**, *3*, 165.
(44) Kim, H.; Jin, W.; Lee, S.; Zhou, P.; Pinnavaia, T. J.; Mahanti, S. D.; Solin, S. A. *Phys. Rev. Lett.* **1988**, *60*, 2168.